Autofluorescence of Condensed Heme Aggregates in Malaria Pigment and Its Synthetic Equivalent Hematin Anhydride (β-Hematin)

Marie-Josée Bellemare,[†] D. Scott Bohle,*[,†] Colin-Nadeau Brosseau,[‡] Elias Georges,[§] Marianne Godbout,[||] Jane Kelly,[⊥] Mara L. Leimanis,[§] Richard Leonelli,[‡] Martin Olivier,[||] and Martin Smilkstein[⊥]

Department of Chemistry, McGill University, 801 Sherbrooke Street West, Montréal, Québec, Canada H3A 2K6; Département de Physique, Université de Montréal, 2900, Boulevard Édouard-Montpetit, Montréal, Québec, Canada H3T 1J4; Institute of Parasitology, McGill University, 21 111 Lakeshore Road, Ste Anne de Bellevue, Québec, Canada H9X 3 V9; Department of Microbiology and Immunology, McGill University, 3775 University Street, Montréal, Québec, Canada H3A 2B4; and Experimental Drug Discovery Lab, Medical Research Service RD-33, VA Medical Center, 3710 SW U.S. Veterans Hospital Rd., Portland, Oregon 97239

Received: November 27, 2008; Revised Manuscript Received: April 16, 2009

The condensed crystalline phase of iron(III) protoporphyrin IX either isolated from parasite culture as malaria pigment (hemozoin) or synthetic equivalent hematin anhydride exhibits a solid-state autofluorescence characterized by an excitation maximum of 555 nm and an emission maximum of 577 nm. The excitation spectrum maximum at 555 nm corresponds to the Q(0,0) band in the absorption spectrum which represents the lowest singlet of the material. This suggests that the fluorescent emission is due to the heme condensed phase. The photoluminescence lifetime of $\tau_f = 2.7 \pm 0.8$ ns as measured at four wavelengths between 550 and 600 nm is in the range of Frankel exciton in porphyrinic condensed phases. The material is shown to have an optical band gap of 2.04 eV characteristic of a semiconductor. Luminescence is markedly dependent upon the degree of hydration and the emission does not seem to be caused by presence of zinc(II) protoporphyrin IX or free-base protoporphyrin IX in the lattice. The autofluorescence can be used for in vivo tracking of hemozoin, for determination of parasitemia levels, and for infection monitoring and possibly for drug screening studies.

Malaria remains a menacing disease with devastating human consequences.[1−3] In spite of the recent control successes in the use and distribution of bed nets[4−7] as well as in the use of endoperoxide antimalarials,[8−12] there is no room for complacency about the return of this scourge. Based upon the time line for the development and spread of chloroquine resistance, there is perhaps a 20-year window for developing new antimalarial drugs and vaccines.[2,3]

Among the unique biochemical targets, the intraerythrocytic formation of the condensed phase of iron(III) protoporphyrin IX known as malaria pigment or hemozoin[13] remains an important one, albeit its poorly understood biochemistry.[14−17] Its pro-inflammatory properties also place hemozoin as a potential agent in the elaboration of a malarial vaccine.[18−22]

From its crystal structure (Figure 1A)[13] hemozoin (HZ) corresponds to chains of propionate linked dimers of five-coordinate high-spin iron(III) protoporphyrin IX, where one of the propionates ligates the iron of reciprocal heme and the second one forms hydrogen bonding with the adjacent dimer.[23,24]

Molecular ferric heme derivatives and their proteins are recognized as efficient quenchers.[25−28] High-spin ferriheme possesses a spin of $S = 5/2$, with all half-filled d-orbitals in the proximity of the porphyrin HOMO and LUMO. This leads to strong mixing between the porphyrin $\pi \rightarrow \pi^*$ and iron $d \rightarrow d$ transitions. It is reflected in broad Q-bands from the absorption spectrum and very weak resonance Raman signal.[28] Also, multiplicity of the Q-bands suggests very strong vibronic coupling among the vibrational levels of the different electronic states (Figure 1B). As an example, methemoglobin possesses a very fast relaxation rate of $\tau_e = 3$ fs inhibiting any measurable luminescence emission.[28] Therefore, black crystals composed of ferriheme are anticipated to be powerful chromophores and not fluorophores.

In this paper, we report the autofluorescence of crystalline HZ from malaria parasites as well as its synthetic analogue, hematin anhydride (HA). Experiments were elaborated such that the photophysical properties observed for these biocrystals could discriminate among the three working hypotheses: coherent superradiance emission, presence of an emitting contaminant, and Frenkel-type exciton in the crystalline lattice. This autofluorescent property was also used to delineate three biological applications relevant to malaria propagation, macrophage activity, and tissue accumulation/pathogenesis. Taken together, these results pave the way for new detection methodologies for studying the development of the parasite as well as for understanding the biochemistry of HZ formation.

Results

Photophysical Measurements. ***Photoluminescence Spectrum and Lifetime Measurements.*** The serendipitous discovery of HZ autofluorescence was first observed on a confocal microscope when a control sample was analyzed for crystals linked with fluoresceinamine. To investigate this observation,

* To whom correspondence should be addressed. E-mail: scott.bohle@mcgill.ca.
[†] Department of Chemistry, McGill University.
[‡] Université de Montréal.
[§] Institute of Parasitology, McGill University.
[||] Department of Microbiology and Immunology, McGill University.
[⊥] VA Medical Center.

10.1021/jp8104375 CCC: $40.75
Published on Web 05/27/2009

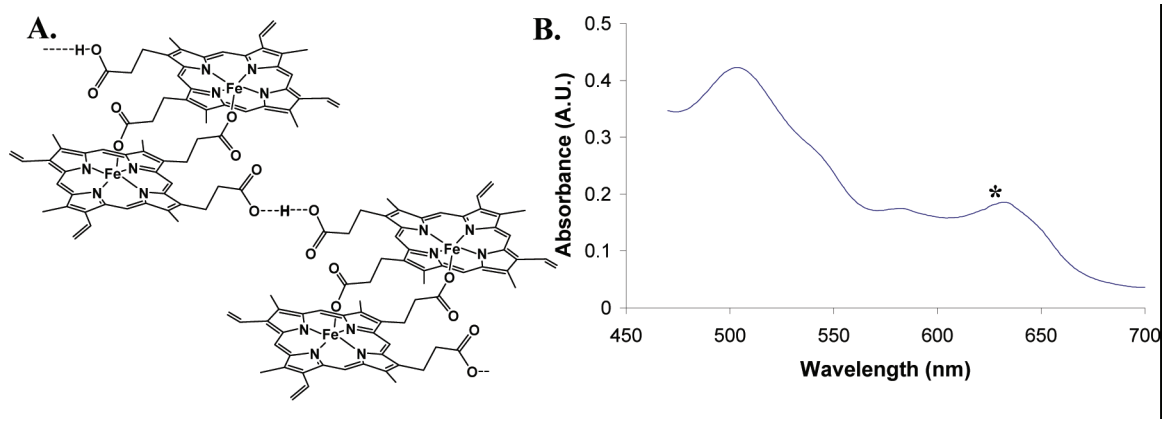

Figure 1. (A) Crystal structure of hematin anhydride. (B) Absorption spectrum of methemoglobin Q-bands. * indicates the charge-transfer band.

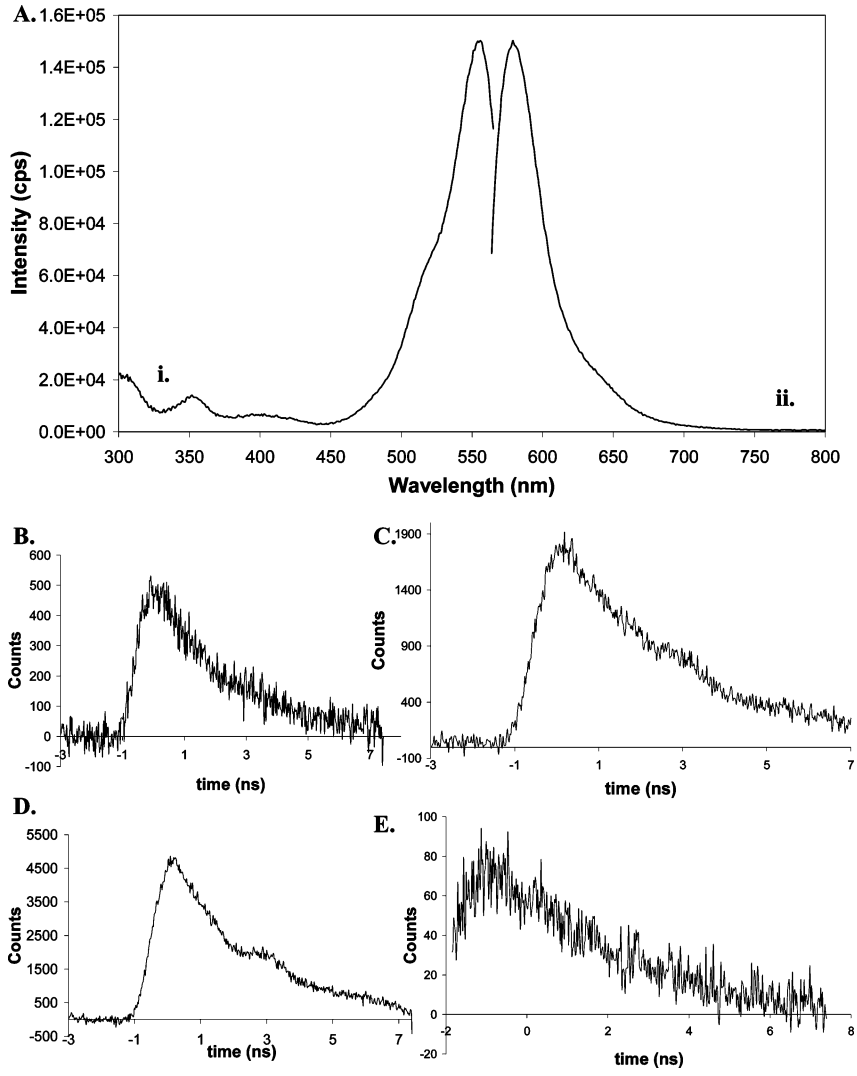

Figure 2. (A) Excitation (i) and emission (ii) spectra of hematin anhydride crystals. Fluorescence decay measurements of hematin anhydride (λ_{ex} = 430 nm). Collections were performed at (B) 550 nm, (C) 575 nm, (D) 580 nm, and (E) 600 nm.

excitation (PLE) and emission (PL) spectra were acquired from crystals deposited between quartz slide and coverslip and brought to the fluorometer. The PLE is almost a mirror image of the PL with a slight shoulder on the PLE, probably from a vibronic contribution, as well as small features of the other absorption bands (Figure 2A). These spectra give maxima of λ_{ex} = 555 nm and λ_{em} = 577 nm.

The radiative lifetimes for these excited states were acquired using a time-correlated single-photon-counting system (TCSPC), Figure S1 in the Supporting Information. Exciting at 430 nm, emission was monitored at four wavelengths between 550 and 600 nm (Figure 2B−D). Using the equation: $y(t) = -e^{-t/\tau}$ and plotting ln(counts) vs time in seconds, the slope becomes $-1/\tau_f$ and the computed lifetime of $\tau_f = 2.7 \pm 0.8$ ns for HA

TABLE 1: Fluorescence Lifetimes Reported for Some Organic Condensed Phases

complex	τ_f		reported radiative mechanism	ref
HA	2.7 ns		to be determined	this work
naphthalene crystals	25 ns		Frenkel exciton	29
anthracene crystals	10 ns		Frenkel exciton	29
tetracene crystal	100 ns		Frenkel exciton	29
Z4[a]	1.75 ns		Frenkel exciton	30
Z64[a]	0.25 ns		superradiance	30
Z128[a]	0.12 ns		superradiance	30
pseudoisocyanine bromide J-aggregate	16 ps	70 ps	superradiance	31
FeTPP aggregates	1.49 ns	7.35 ns	fast component is attributed to intermolecular interaction in formed aggregate	32
B820[b]	590 ps	19.7 ns	fast component from superradiance and slow from exciton recombination	33
LH-2[b]	986 ps	10 ns	fast component from superradiance and slow from exciton recombination	33
LH-1[b]	680 ps	8.4 ns	fast component from superradiance and slow from exciton recombination	33

[a] Zinc(II) 5,15-bis(3,5-bis(octyloxy)phenyl)porphyrin *meso, meso* linked arrays of 4, 64, and 128 porphyrins. [b] Photosynthetic subunit of *Rhodobacter sphaeroides*.

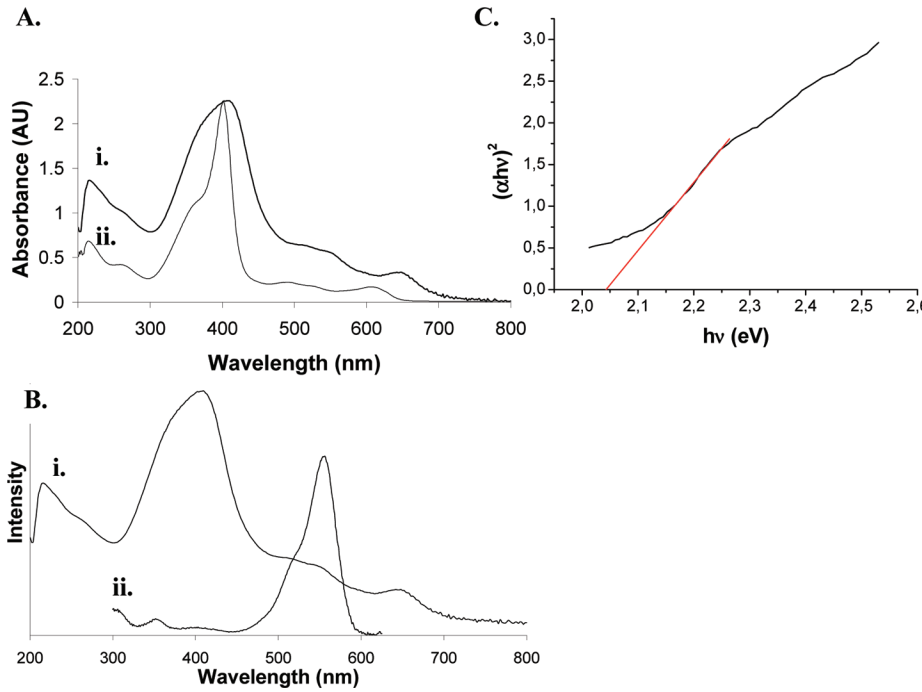

Figure 3. Q(0,0) band is responsible for the luminescence emission. (A) Absorption spectra of (i) hematin anhydride in KBr and (ii) monomeric hematin in 2% SDS solution, (B) absorption (i) and excitation (ii) spectra of hematin anhydride, and (C) Tauc plot for optical band gap determination.

is obtained. This time frame is in the lower limit (Table 1), of an exciton recombination of the Frenkel-type observed in organic crystalline materials (Table 1). This could be expected as the crystals are composed of paramagnetic high-spin ferriheme and therefore very short excited lifetime is anticipated. If the process was that of a coherent superradiance, a lifetime of a few picoseconds or faster was anticipated.

Excitation Maxima Matches the Q(0,0) Band. The absorption spectrum of HA measured on a diode array spectrophotometer as a suspension in KBr is shown in Figure 3A. It is contrasted with a solution of nonaggregated hematin in 2% SDS. Clearly, the Soret band (~400 nm) is broader and split, the Q-bands (480−580 nm) are more intense, and overall the spectrum is shifted to the red. These spectral changes from isolated individual molecules in solution to those of a crystalline phase are a characteristic signature for a molecular exciton within the crystalline lattice.[29,34]

In order to see if one of the HA electronic transitions is responsible for this luminescence, the absorption spectrum is compared to the PLE. The maximum of the excitation spectrum coincides well with the Q(0,0) band which corresponds to the lowest porphyrin $\pi \rightarrow \pi^*$ singlet (Figure 3B).[26,27,35] This supports the hypothesis that the observed fluorescence emission is one of the porphyrin material and not from an impurity. Also, HA is found to obey Kasha's rule which states that the radiative transition in a given spin manifold always occurs from the lowest excited state.[36] Coming from the lowest singlet, this photoluminescence can be characterized as fluorescence.

The optical band gap "E_g" was obtained calculated using the equation: $\alpha = A(h\nu - E_g)^n/h\nu$ where α is the optical absorbance, A and n are constants, and $h\nu$ is the photon energy. For allowed direct transition $n = 1/2$ and for allowed indirect transition $n = 2$.[37−39] Since maximum excitation falls on the Q(0,0) band, n was chosen as $n = 1/2$, and from the Tauc plot, the optical

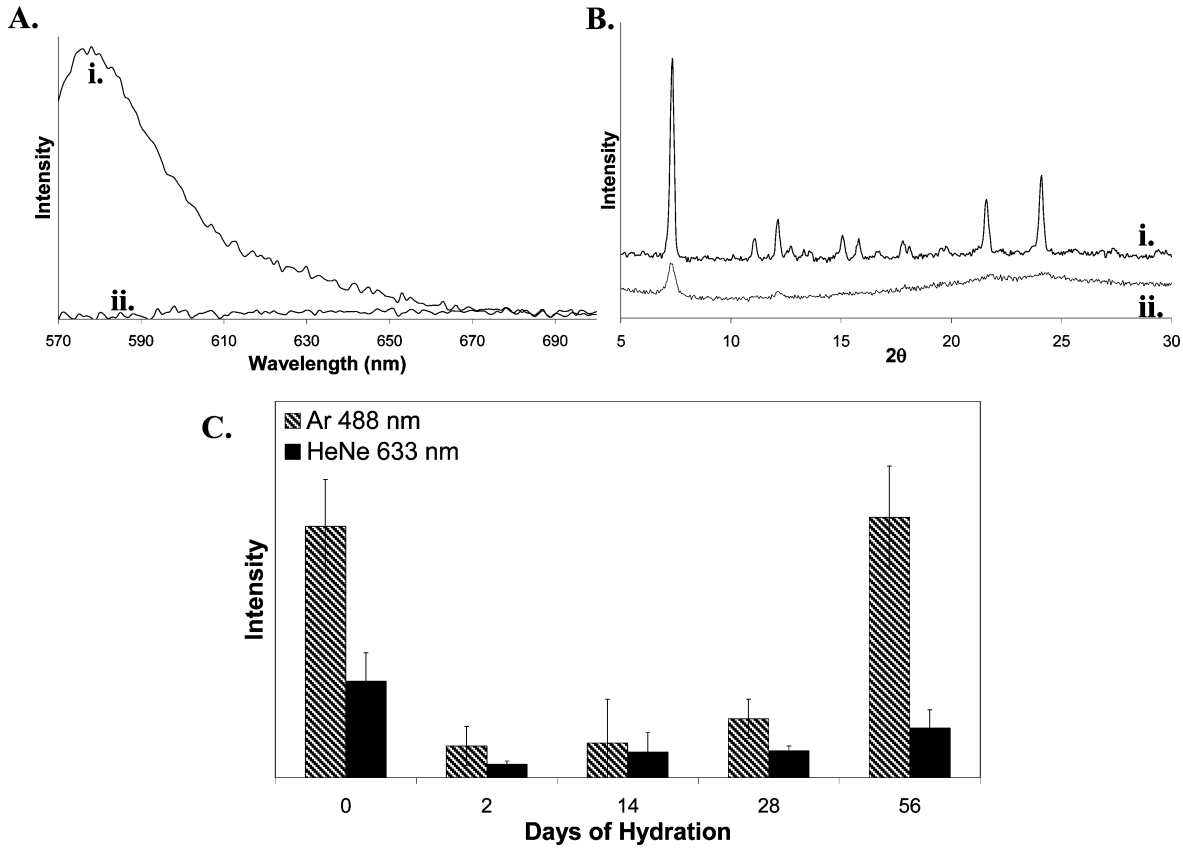

Figure 4. Crystalline material is required for luminescent emission. (A) Emission spectra and (B) powder XRD pattern of (i) crystalline vs (ii) amorphous hematin anhydride (HA) prepared by uncontrolled acid-catalyzed HA dehydration. (C) Intensity of the fluorescence emission for hematin anhydride as a function of the days of hydration using the 488 nm line of an Ar laser or a 633 nm HeNe laser.

band gap was extrapolated to $E_g = 2.04$ eV (Figure 3C). This value falls exactly in the range recognized for semiconductors of ~0.5−3.5 eV.[40,41]

Quantum Yield. The quantum yield of the autofluorescence may be useful in distinguishing between the fluorescence mechanisms. Unfortunately, all applications of the reported methods for solid samples have failed to give reliable values so far. For example, the Strickler−Berg approximation[42] was tried with the integration of the Q(0,0) band and the experimentally determined value of τ_f. The computed value of $\Phi = 0.22$ is too high from expected value. This suggests that this process involves intermolecular interactions as the Strickler−Berg analysis usually gives calculated values within >90% experimental values for molecular compounds only.[42−45] Also, the fact that this photoluminescence cannot be observed with a standard fluorescence microscope and that no signal was observed with the integrating sphere suggest a per heme quantum yield lower than 10^{-6}. Although these quantum yields are low the fluorescent signal is nevertheless easily detected with a laser confocal microscope. This is likely to be due to the relatively high the concentration of fluorophores in solid hematin anhydride.

Photoluminescence and Crystalline Network. ***Hydration of Hematin Anhydride and the Crystal Mosaic Modulate the Luminescence.*** For many solid-state porphyrin arrays, the major factor regulating the fluorescent emission is the nature of the short- and long-term order of the lattice.[30,34,46−49] Similar behavior is observed for HA. While crystalline samples of HA are luminescent, the more amorphous material (as determined by X-ray powder diffraction) is poorly luminescent (Figure 4A,B).

HA can reversibly absorb up to 14% of its mass in water.[50] This hydration process was found to affect the crystalline lattice.[50] A similar effect was observed with the photoluminescence. Freshly prepared and thoroughly dried crystals were deposited in a hydrating chamber, and the effect on luminescence was monitored over days of hydration. The strongest luminescence was observed for either the fully hydrated or completely dried HA (Figure 4C). When the crystals were completely dried, the lattice network was formed and luminescence was emitted. As the crystalline network was disturbed by an uneven degree of hydrations, photoluminescence was affected. Crystallinity and photoluminescence were recovered upon complete hydration. This result again suggests that the fluorescence emission arises from intermolecular interactions such as exciton recombination.

Cocrystallite Contamination. ***Detection of PPIX in Starting Material and Synthesized Crystals.*** It is known that about 0.01% of protoporphyrin IX free-base (PPIX) and Zn(II) protoporphyrin IX (ZnPPIX) occupies the heme site in normal human hemoglobin.[51,52] The amount of zinc metalation of PPIX in general reflects the iron levels and/or nutrition/status of the individual, and there is a fluorometric method for detecting the level of Zn(PPIX) in red blood cells that is used as a clinical anemia assay.[53,54] However, as hemin is extracted from blood and recrystallized using glacial acetic acid and HCl, the Zn(II) is liberated and often only free-base PPIX can be observed.[55−57] Indeed, when starting material, crystalline bovine hemin (Fluka) was dissolved and diluted in μM range with NaOH (20 mM): SDS 2% aqueous solution, the PPIX emission ($\lambda = 626$ nm) was observed at excitation wavelength of 405 nm (Figure 5A). If the solution was concentrated, the signal was quenched by the greater number of ferriprotoporphyrins present. If HA from both preparations (acid-catalyzed and anhydrous base, see Experimental Section) is dissolved in the same heme concentration (10 μM) and same solvent system, the measured PPIX peak will be the same intensity showing that PPIX is carried through

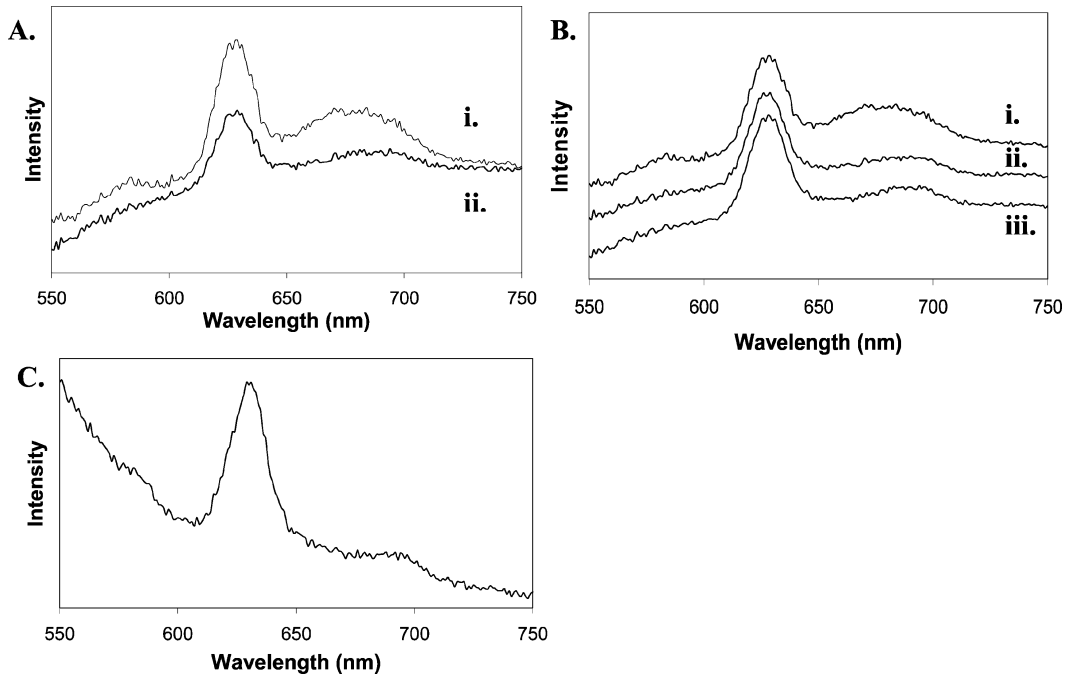

Figure 5. Protoporphyrin IX (PPIX) is carried through hematin anhydride (HA) synthesis: (A) emission spectrum of PPIX in (i) 9.9 μM and (ii) 19.8 μM hemin solution; (B) PPIX signal observed in 10 μM solutions (heme content) of starting material (i) hemin, (ii) acid-catalyzed HA, and (iii) anhydrous base HA; (C) PPIX signal observed with natural hemozoin produced from *Plasmodium falciparum*, Dd2 strain. All spectra were performed for crystals degraded in aqueous 2% SDS:20 mM NaOH and were acquired from 500 to 750 nm when exciting at $\lambda = 405$ nm.

HA synthesis (Figure 5B). Finally, if natural hemozoin (HZ) produced by malarial parasite *Plasmodium falciparum* is dissolved in NaOH (20 mM):SDS 2% solution, the PPIX emission was observed when exciting at $\lambda = 405$ nm (Figure 5C). This result suggests that the parasite also incorporates PPIX in the heme crystals.

Hemin Compared to HA. When the starting material, crystalline hemin, was investigated using a Raman microscope, weaker fluorescence was observed if compared to the one collected for HA even if they possess the same PPIX content (Figure 6A). As they share different crystal structure, this fluorescence discrepancy is consistent with the presence of a molecular exciton in the lattice being responsible for the photoluminescence.

Doping the Crystals with PPIX. PPIX-doped HA crystals were synthesized using the acid-catalyzed method and the PPIX content was verified by MALDI-TOF. Uniform PPIX fractions were observed throughout the whole crystals as the PPIX peak of the same relative intensity with each successive laser ablation until complete crystal disintegration. The doped crystals also showed stronger fluorescence intensity with respect to PPIX content, although not exactly in the same emission range (Figure 6B−D). The PPIX spectrum obtained measured with the Raman microscope presents three peaks, $\lambda = 656$ nm, $\lambda = 689$ nm, and $\lambda = 714$ nm, while the spectrum of HA has two bands at $\lambda = 673$ nm and $\lambda = 706$ nm when excited with the 514 line of an Ar laser.

Fluorescence of Hematin Anhydride from Purified Hemin. To complete this contamination investigation, the hemin starting material was purified by column chromatography and recrystallization.[55,58] The resulting HA crystals were luminescent, although no PPIX signal could be detected when degraded in 2% SDS:20 mM NaOH (Figure 7).

Biological Applications. ***In Vivo Tracking.*** The autofluorescence of hemozoin and its synthetic analogue allows its visualization in vivo without the requirement of a fluorescence tag or the addition of an exogenous dye (Figure 8). The crystals were visualized in the phagosome of a macrophage, in liver filtering capsules[59] and in infected red blood cells.

Parasitemia Level Determination. Visualization of hemozoin crystals inside red blood cells opens the possibility for a parasitemia level determination by fluorescence (Tables 2 and 3). The percentage of infected cells were determined microscopically by counting at least 1000 red blood cells, using thin Giemsa-stained smears and the fluorescence emitting cells of nonstained slides. Giemsa staining had no impact on the fluorescence counts. The counts were generally slightly lower for the fluorescent method as compared to the counts from the Giemsa staining. The requirement for the presence of hemozoin in the fluorescence method was confirmed when synchronized slides were used and a lower score was obtained observed for the rings stage. It should be noted that synchronization is not 100%, and therefore ring stages will be a mix of early, mature, and late-stage rings; additionally, there may be some early trophozoites as well (Tables 2 and 3). In general, the criteria used for parasite stagging is done using the visual presence of pigment (HZ) as a marker for early trophozoites. Although evidence shows that hemoglobin digestion takes place in the ring stage,[60] this may go unnoticed to the human eye, as sufficient HZ accumulation is necessary to detect it by microscopy. Additionally, ring-stage parasites share HZ magnetic properties as previously shown by magnetic disposition microscopy.[61] While Giemsa stains the parasite's DNA, allowing visualization of all erythrocytic stages, from merozoites to schizonts, fluorescence relies on the presence of HZ and therefore can only count the later stages. The low percentages obtained with the ring-synchronized slides may come from early trophozoites already present in the smears. However, these results show that this autofluorescence property of HZ can still be used for parasitemia detection and quantification.

Infection Monitoring. Another research tool which could benefit from this photoluminescence property would be infection

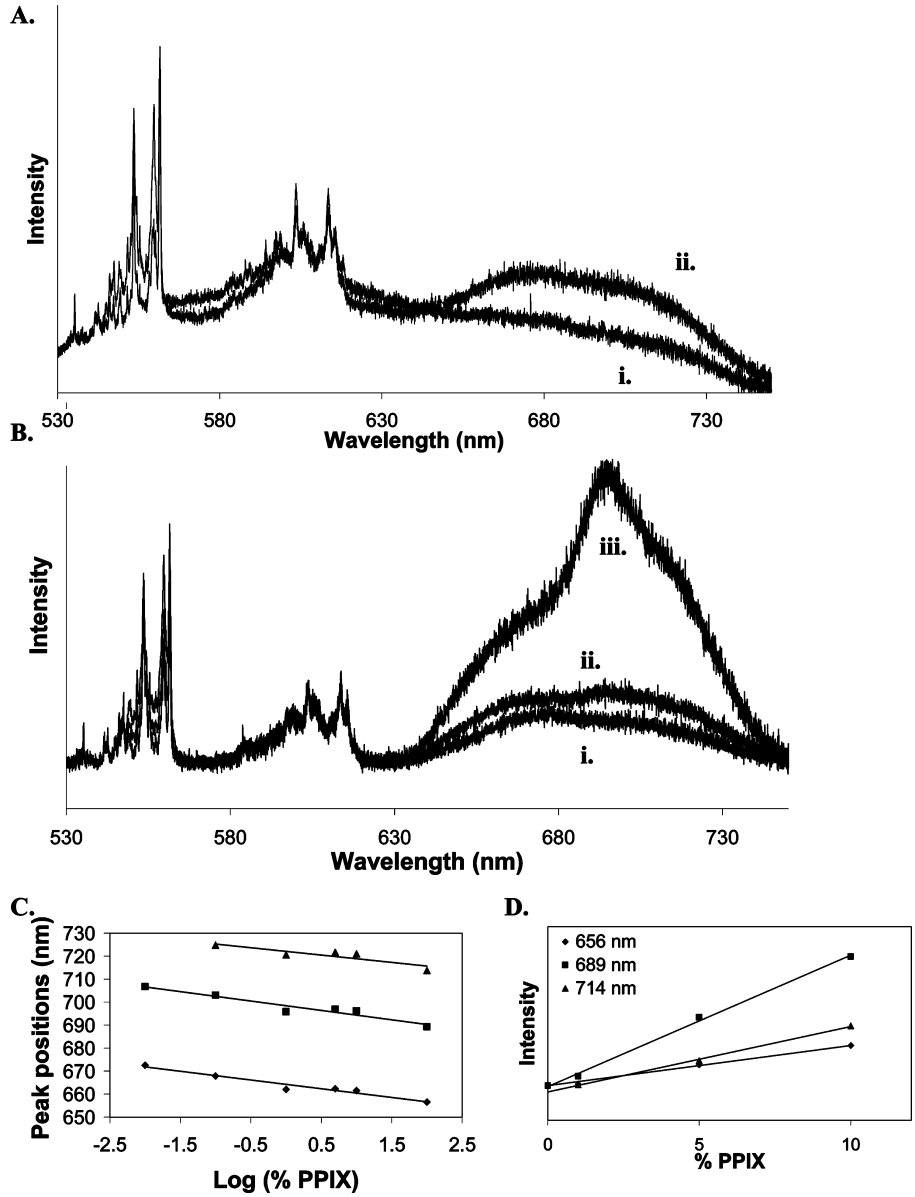

Figure 6. (A) Resonance Raman and fluorescence spectrum of (i) crystalline hemin compared with ii. HA. (B) Variation in Raman spectrum of HA crystals doped with free-base PPIX: (i) control sample, (ii) with 0.1% PPIX, and (iii) with 1% PPIX; (C) peak displacement; and (D) peak intensity with respect to PPIX content.

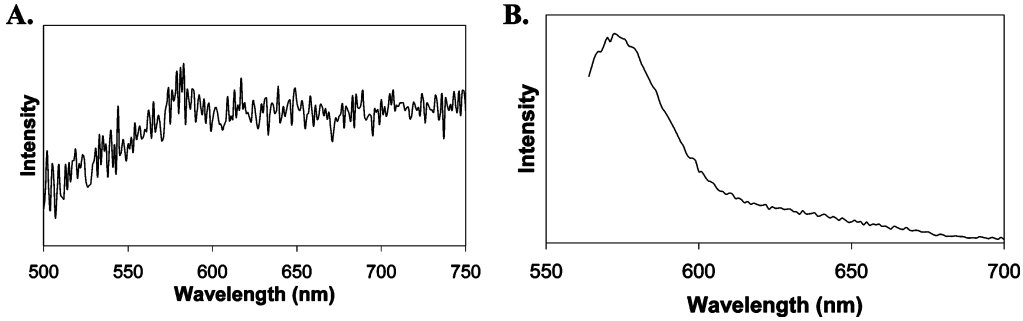

Figure 7. Photoluminescence spectra of purified acid-catalyzed HA: (A) crystals degraded in 2% SDS:20 mM NaOH solution 9 μM (heme content) exciting at $\lambda = 405$ nm, and (B) crystalline sample exciting at $\lambda = 555$ nm.

tracking. Five mice were inoculated with *Plasmodium chabaudi adami* and infection level determined by Giemsa staining in parallel with fluorescence measurement (Figure 9).

Discussion

Hematin anhydride autofluorescence was simultaneously discovered during confocal experiments in two of our separate laboratories. In one set of experiments the crystals were tagged with a long-chain fluorescent probe to determine drug adhesion to their growing crystal faces. These black paramagnetic chromophores composed of high-spin Fe(III) porphyrin were expected to be effective quenchers and were not expected to fluoresce.[23] Therefore, the probes were con-

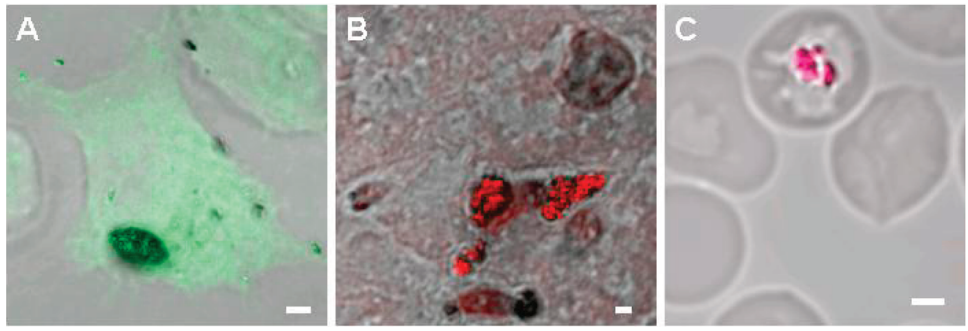

Figure 8. Confocal images of hemozoin and synthetic analog in vivo: (A) acid-catalyzed hematin anhydride engulfed by macrophage; (B) acid-catalyzed hematin anhydride in a mouse liver; and (C) *Plasmodium falciparum* hemozoin from a late trophozoite, strain 7G8. Images were acquired on a Zeiss LSM-150 confocal microscope using the 488 nm line of an Ar laser (A) or a 633 nm HeNe laser (B and C). Bars = 2 μm.

TABLE 2: Parasitemia % As Represented from Both Fluorescence and Giemsa-Stained Samples of Nonsynchronized in Vitro Cultivated *Plasmodium falciparum* Strains 3D7, 7G8, and FCR-3

		% parasitemia	
strain	sample no.	fluorescence	Giemsa
3D7	1	13.82	18.17
	2	11.54	9.24
	3	6.43	9.54
FCR-3	1	19.21	29.10
	2	18.33	23.55
	3	9.55	13.78
7G8	1	17.73	18.00
	2	3.31	3.35
	3	3.46	1.98

TABLE 3: Parasitemia % As Represented from Both Fluorescence and Giemsa-Stained Samples of Synchronized in Vitro Cultivated *Plasmodium falciparum* Strains 3D7 and FCR-3

			% parasitemia	
strain	sample no.	description	fluorescence	Giemsa
3D7	1	trophozoites and schizonts	3.71	4.04
	2	rings and early trophozoites	3.61	4.78
	3	trophozoites	5.18	6.31
	4	rings and early trophozoites	3.12	4.72
	5	trophozoites and schizonts	2.08	2.66
FCR-3	1	trophozoites	5.03	5.58
	2	rings and early trophozoites	6.37	7.62
	3	trophozoites	7.05	8.16
	4	rings and early trophozoites	3.53	8.22
	5	trophozoites	4.34	4.23

structed with long aliphatic spacing units between the drug and the fluorophore. Nevertheless, during control experiments the HZ autofluorescence reported here became obvious.

HZ autofluorescence has been observed before, but it has been either misassigned or not examined in detail. Schwarzer and co-workers used the "red fluorescence associated with heme (HZ, RBC)" in studies of oxidative hemozoin degradation inside the macrophage phagosome and suggested that the photoluminescence could be related to the "red fluorescent haem derivative" observed by Nagababu and Rifkin.[62,63] Carney and co-workers also followed HZ in macrophages using this autofluorescence property; this time, the fluorescence signal was attributed to HZ.[64] Subsequently, Wood and co-workers suggested

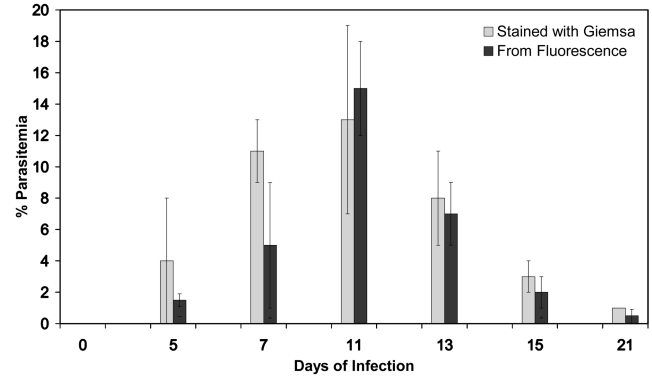

Figure 9. Mouse infection tracking comparing Giemsa staining and hemozoin fluorescence.

that HZ autofluorescence was responsible for the band enhancement observed in their Raman spectra at very specific wavelengths but did not investigate the phenomenon further.[65,66] At the outset, a list of working hypotheses was generated to explain this phenomenon by mechanisms, such as superradiance, ZnPPIX and PPIX contamination, and migration of an exciton through the porphyrin lattice.

Cooperative spontaneous emission (superradiance) is encountered in porphyrin arrays, where molecules radiate in phase, and the radiative rate is enhanced by the number of cooperative chromophores.[30,33,67] For HA, the relatively long fluorescence lifetime, $\tau_F = 2.7 \pm 0.8$ ns rules out a superradiative excited state since shorter lifetimes, typically in the picosecond range, are required so that emission can compete with nonradiative decay (Table 1). Composed of paramagnetic high-spin ferriheme, if HZ autofluorescence would originate from superradiance, a lifetime in the few picoseconds or faster would be anticipated.

The contamination hypothesis stems from the fact that ZnPPIX and PPIX are present in ca. 0.01% proportion in normal blood hemoglobin.[51,52] Their fluorescence is such that only a minute amount can generate a detectable signal in solution.[26,53,54,56] This was demonstrated here in very dilute hemin solutions as fluorescence PPIX peaks appeared in 10 μM hemin. (Figure 5A) In the condensed phase, fluorescence from PPIX and HA have quite different signatures (Figure 6B−D). Deprived of the iron center, PPIX exhibits a much stronger luminescence as different conditions had to be used for pure PPIX under both the confocal and Raman microscope to not saturate the CCD with respect to HA (data not shown). Therefore, the luminescence intensity was proportional to the PPIX content in the HA-doped crystals. Also, under the Raman microscope operating with the 514 nm line of ar Ar laser, PPIX exhibits three peaks while HA possesses 2 bands.

A much weaker fluorescence was observed for the starting material, crystalline hemin with respect to HA (Figure 6A), although when the HA crystals are dissolved in a basic surfactant solution, the PPIX present in the starting material is carried through the condensed phase with a similar concentration (Figure 5B). Finally, when rigorously purified hemin is used in the synthesis of HA, there is no PPIX fluorescence detected when the crystals are degraded in SDS:NaOH; and the crystalline HA prepared from this purified hemin still emits with similar intensity (Figure 7). These results demonstrate that PPIX is not responsible for the observed autofluorescence of HZ. It does not completely remove the possibility that some other contaminant contributes to the autofluoresence but at this time we have been unable to identify any candidate molecules which would not give a mass spectroscopic signature, and would be present in both synthetic and in vivo HA crystals. Application of Occam's razor supports the most direct hypothesis that the fluorescence is due to HA itself.

Monomeric porphyrins possess rich photoluminescence properties due to their extended π systems,[26] but their fluorescence emission tends to decrease drastically as they aggregate in a irregular manner.[68−73] However, in crystalline arrays of free-base or diamagnetic porphyrins, new photoluminescence properties emerge from strong intermolecular interactions.[30,34,46−49,74] There is, however, little precedent for these trends in paramagnetic porphyrin arrays.[49,75,76] Photoconductivity has been reported for crystalline hemin,[75,76] and the fluorescence of *meso*-tetraphenylporphyriniron(III) chloride (FeTPPCl) aggregates has been investigated.[32]

HA possesses a large delocalized π system which is thought to be responsible for its very intense third harmonic signal.[77] The porphyrin planes of adjacent dimers in the crystal packing are only 3.79 Å away from each other (SI.2A). Also, tunnelling throughout the crystal lattice could be anticipated as porphyrinic arrays appear along the *b* axis. (SI.2B) With an optical band gap of $E_g = 2.04$ eV, characteristic of semiconductors,[40,41] exciton migration along the crystalline lattice was anticipated.

Confirmation that this photoluminescence could be generated by exciton recombination in the lattice comes from the spectral analysis. When the absorption spectra of the monomer and the crystal are compared, the Soret band is broader and split, the Q-bands are enhanced, and the spectrum exhibits bathochromic shift characteristics of an exciton migration in the ensemble[29,34] (Figure 3A). As for other crystalline porphyrins,[30,34,46,47] absorption and excitation spectra of HA differ: the maximum excitation spectrum falls exactly on the Q(0,0) band which corresponds to the $S_0 \rightarrow S_1$[26,27,35] (Figure 3B). These analyses converge with the hypothesis that the observed photoluminescence is a fluorescence emission of the crystalline material and not from an emitting impurity.

HA autofluorescence can only be observed for crystalline material (Figure 4A,B). It is independent of the method used to prepare it, as well as crystal size (data not shown). However, the crystals have to be either extensively dried or fully hydrated for the fluorescence to be observed, suggesting the requirement of an undisturbed lattice (Figure 4C).[50] All of these results suggest an exciton migration through the crystalline lattice of HA, although the exciton recombination process responsible for the observed photoluminescence remains speculative. Complete investigation of this phenomenon should be achieved with quantum yield determination, transient absorption and emission experiments, and high-pressure fluorescence studies.

The applications of this intriguing fluorescence property are numerous. Although on a per heme basis the signal is weak, the net per crystal signal is detectable and the possibility of measuring the luminescent emission in the red and even far red allows for tracing HZ and its synthetic analogue in live tissues. Thus, HZ autofluorescence in infected red blood cells, liver, and macrophages has been observed. The level of parasitemia determinations and infection tracking compare well with results obtained by the conventional Giemsa staining. This confirms that HZ and HA can be visualized inside biological samples without any staining which allows for a noninvasive and faster determination of parasitemia. The limitation at this time is that late-stage parasites are easily detected using this fluoresence method, however, ring-stage parasites, which are detected in peripheral blood of *Plasmodium falciparum* infections, may not be detected. The presence of later-stage parasites may appear in peripheral blood in more advanced infections, indicative of high total parasite biomass due to the sequestration of *P. falciparum* in the microvasculature.[78] Conventional Giemsa stain in combination with RDT's is optimal for rapid early detection of ring-stage parasites, as a patient presenting with later-stage parasites in the peripheral blood may be indicative of a more critical clinical case. Autofluorescence of HA is therefore an important tool for monitoring crystalline hemozoin formation and, possibly, drug interference.

Experimental Section

Hematin Anhydride Synthesis. Detailed procedures and characterization data are given elsewhere.[79] Briefly, either one of the following techniques was used.

Anhydrous Base Dehydrohalogenation Method. Hemin (Fluka Chimie, Buchs, CH-9471 Switzerland) (0.8 mmol, 500 mg) is transferred in an inert atmosphere box. Sufficient 2,6-lutidine (10 mL) is added to dissolve it completely. The solution is diluted by the addition of 1:1 methanol:dimethyl sulfoxide (100 mL). The flask is then sealed, wrapped in aluminum foil, and taken out of the box. It is allowed to stand undisturbed for anywhere between 2 weeks to 15 months depending on the desired yield. The flask is then opened and the black mixture is centrifuged at 7000 rpm for 1 h, and the supernatant decanted. The crystals are then washed once with $NaHCO_3$ (0.1 M) for 3 h. The final washes are with alternating Milli-Q purified water and methanol for three times each. The sample is dried in vacuum oven at 100 °C overnight.

Acid-Catalyzed Thermal Annealing Method. Hemin (0.8 mmol, 500 mg) is dissolved in degassed NaOH (0.1 M, 100 mL) during 30 min with mild stirring. Propionic acid is added dropwise over a 20 min period until a pH of about 4 is achieved. The mixture is heated at 70 °C for 18 h. After cooling, the solid is separated and washed as follows: three $NaHCO_3$ (0.1 M) washes for 3 h are alternated with Milli-Q water. Finally, MeOH and Milli-Q water are alternately used to wash a final three times. The sample is then dried in a vacuum oven overnight over phosphorus pentoxide. All hematin anhydride samples were characterized by XRD, IR, and FEG_SEM.

Powder X-ray Diffraction (XRD). Powder diffraction data were collected on a Siemens D5000 X-ray diffractometer using a Cu Kα radiation source ($\lambda = 1.514$ Å). Samples were pulverized and transferred into a 1 mm diameter glass capillary. The latter was aligned with the beam but was not rotated, and held by a polypropylene capillary holder.

Attenuated Total Reflectance-Infrared spectroscopy (ATR-IR). Spectra were obtained as the crystals were pressed on a diamond MIRacle ATR cell from PIKE Technology installed on a Perkin-Elmer FTIR BX System and running with Spectrum software.

TABLE 4: Solvent Systems Used during the Column Purification of Hemin

solvent volumes	methanol	acetonitrile	acetic acid	pyridine
system1	480	480	2	80
system2	120	360	1	40

Field Emission Gun Scanning Electron Microscopy (FEG_SEM). SEM pictures were acquired using a Hitachi S-4700 FE_SEM. The samples were coated with Au/Pd of about 4 Å thickness prior to visualization at 2 kV and 10 μA.

Protoporphyrin IX Free Hemin. Hemin was purified from PPIX and ZnPPIX using a modified method reported by Dixon and co-workers.[58] Two solvent systems were prepared as in Table 4.

Hemin (20 mg, 31 μmol) is dissolved in 5 mL of system 1 in a vial wrapped in aluminum foil. A silica gel column is prepared and flushed with system 1 solvent. The hemin sample is injected and eluted with solvent system 2. The first 10 mL of colored eluent from main band were discarded. After switching to solvent system 1, the remainder of this band was collected and filtered and the solvents were removed in vacuo. Recrystallization of the resulting hemin followed directly the method reported by Fischer.[55] Briefly, crude recovered hemin, ~15 mg, was dissolved in pyridine (150 μL). Chloroform (240 μL) is added to an aluminum foil wrapped flask and allowed to mix for 15 min. The solution is then filtered and the pyridine-insoluble materials are rinsed with 90 μL of chloroform. A mixture of glacial acetic acid (2.1 mL), saturated aqueous NaCl (30 μL), and concentrated HCl (24 μL) is brought to a boil and then removed from the heat source, to which the filtered hemin solution is added as a steady stream with constant stirring. Upon standing 12 h, the recrystallized hemin is recovered by centrifugation and washed with 400 μL of 50% aqueous acetic acid, 800 μL of Milli-Q water, 100 μL of ethanol, and 100 μL of diethyl ether. Yield: 35−67%. The best yields are obtained when the mobile phase from the column was not completely dried, leaving hemin already dissolved in pyridine. The resulting hemin has no fluorescence upon dissolution in 2%SDS/20 mM NaOH at concentration of 9 μM or lower, with an excitation of 405 nm and measuring from 500 to 750 nm.

Fluorescence Spectroscopy. A few crystals were spread on a quartz microscope slide and the quartz coverslip was sealed with nail polish. Using a front-loading solid sample holder model 1933, spectra were acquired on a Jobin-Yvon Fluoromax 2 equipped with a Xe lamp, double grating, PMT detector, and running with Datamax software.

Absorption Spectroscopy. Absorption spectra were collected with an 8452A diode-array spectrophotometer driven by a HP 89532 UV/vis general scanning software as the solid of interest was pulverized in a KBr matrix.

Confocal Imaging. Samples were prepared on microscope slides and observed using the single-track configuration of a Zeiss LSM-150 confocal microscope running with Zeiss software. Keeping the bright field open on one channel, images were acquired either with the 488 nm line of an Ar laser, collecting using the long path filter for $\lambda > 505$ nm (LP505) (green band) or with a 632.5 nm HeNe laser and collecting from 655−700 nm (red band). In order to minimize scattering induced by the red blood cells, a thin film of Immersol 518F (Carl Zeiss, Oberkochen, Germany) was spread between slide and coverslip.

Fluorescence Lifetime Measurement. Fluorescence lifetimes were acquired using time-correlated single photon counting (TCSPC) (Figure SI1, Supporting Information). A schematic of the system is depicted in Figure SI1. Sample was excited at 430 nm as the signal from a Titanium Sapphire laser (Coherent, Mira at 860 nm, ~1 W, 2 ps) which is pumped by a Coherent laser (Coherent, Verdi V-10 at 532 nm, 10 W) was passed through a frequency doubling β-BaB_2O_4 (BBO) crystal. Photon emission was captured by a fluorometer (Princeton Instrument, Trivista) equipped with photomultiplier (PMT) detector (Hamamatsu, R943-02) and PMT amplifier (Stanford Research, SR445A). The measured signal was transmitted via constant fraction discriminator (CFD) (Ortec, 584) to the time amplitude converter (TAC) (Ortec, 567) along with the trigger for the excitation (laser).

Resonance Raman spectroscopy. Raman spectra were acquired using an inVia Renishaw spectrometer with a charge-coupled detector running with WIRE 2.0 software. A few hematin anhydride crystals were deposited on a microscope slide and excited with three laser lines: argon 514 nm, HeNe 632.5 and diode array 785 nm. All measurements were performed at room temperature and the experimental data are considered to be accurate to within ± 1 cm^{-1}.

Hydration Study. Freshly prepared thoroughly dried hematin anhydride crystals from both methods were deposited in a hydrating chamber, and the effect on luminescence was monitored with days of hydration. The hydrating chamber consisted of a desiccator to which desiccant was replaced by deionized water which was refreshed every second day.

Hematin Anhydride Doped with Free-Base Protoporphyrin IX. Acid-catalyzed procedure was performed as control hemin from (Fluka) was replaced by hemin purified by chromatography or hemin (Fluka) contaminated with 0.01, 0.1, 1, 5, and 10% PPIX molar ratio. PPIX content was verified by MALDI-TOF as a uniform PPIX peak is observed during successive laser ablations.

In Vitro Parasite Culture. *Plasmodium falciparum* strain 3D7, FCR-3, and 7G8 (kindly provided by Dr. A. Cowman at The Walter and Eliza Hall Institute of Medical Research, Melbourne 3050, Australia) was grown in continuous culture as previously described by Trager and Jensen.[80] Washed human erythrocytes (type B^+) from freshly drawn blood were suspended in culture medium (RPMI-1640 from Gibco supplemented with 0.5% Albumax II, 0.32 mM hypoxanthine, 2 mM L-glutamine, 25 mM HEPES, 24 mM sodium bicarbonate, 11 mM glucose) at 5% hematocrit and inoculated with infected erythrocytes. The flasks were incubated in ten milliliters of parasite suspension at 37 °C in a T-25 tissue culture flask by candle jar method[80] FCR-3 was grown in 5% CO_2 incubator. Cultures underwent daily changes of medium and were synchronized by sorbitol lysis at the ring stage.[81] The percentage of infected cells (parasitemia) was determined microscopically by counting at least 1000 red blood cells, using thin Giemsa-stained smears.

Macrophage Cells (Mϕ) and Culture Conditions. The murine Mϕ cell line B10R, derived from the bone marrow of B10A.Bcgr (B10R) mice,[82] was kindly provided by Dr. Danuta Radzioch (McGill University, Montréal, Canada). Cells were maintained in DMEM (Life Technologies, Rockville, MD) supplemented with 10% heat-inactivated FBS (HyClone Laboratories, Logan, UT) plus 100 μg/mL streptomycin and 2 mM L-glutamine at 37 °C and 5% CO_2. Mϕ were seeded in 12-well plates on a round coverslip at a density of 10^5 cells, and thereafter hemozoin (HZ) at a concentration of 3 mg/mL was incubated with Mϕ for 15−60 min. Uningested HZ was washed from cell culture with PBS and HZ-laden cells then prepared on slides with PremaFluor mounting media (Thermo Electron Corporation, Pittsburgh, PA) for confocal visualization.

Mice. Female Balb/c mice, 6−8 weeks old, were purchased from Charles River Laboratories (St. Constant, QC, Canada). All animal experiments were performed in accordance with the guidelines of the Canadian Council for Animal Care.

Parasites and Experimental Infections. The *Plasmodium chabaudi adami* DK strains derived from two different isolates.[83] Female BALB/c mice, 4−6 weeks old (Charles River), were infected with 10^5 parasitized red blood cells (PRBC) by the i.p. route. Parasitemia was measured daily in methanol fixed tail blood smears stained with a 10% Giemsa solution in PBS.

Hematin Anhydride Accumulation in Liver. Female BALB/c mice, 6−8 weeks old (Charles River), were injected with hematin anhydride suspension in endotoxin free PBS (250 μg in 250 μL). The mice were killed 6 h later and livers were retrieved. Slides were prepared from microslices of paraffin blocks and cells were stained with hematoxylin followed by eosin.

Acknowledgment. We gratefully acknowledge Mirela M. Barsan and Jacynthe Laliberté from the McGill Chemistry and Life Sciences Complex Imaging Facility, respectively, for advice and assistance with some of the measurements. Support from NSERC (D.S.B., E.G.), CRC (D.S.B.), CHIR (D.S.B., M.O.), and the Veterans Administration (J.K. and M.S.) is gratefully acknowledged.

Supporting Information Available: Two pages with details of the lifetime measurements and exciton transmission pathways. This material is available free of charge via the Internet at http://pubs.acs.org.

References and Notes

(1) WHO, The World Malaria Report 2008, www.who.int/malaria.
(2) Maher, B. *Nature* **2008**, *451*, 1042–1046.
(3) Looking Forward - Roll Back Malaria; Roll Back Partnership Secretariat, Geneva, 2004; p 16.
(4) Grabowsky, M. *Nature* **2008**, *451*, 1051–1052.
(5) Okiro, E. A.; Hay, S. I.; Gikandi, P. W.; Sharif, S. K.; Noor, A. M.; Peshu, N.; Marsh, K.; Snow, R. W. *Malar. J.* **2007**, *6*, 151–161.
(6) Bhattarai, A.; Ali, A. S.; Kachur, S. P.; Martensson, A.; Abbas, A. K.; Khatib, R.; Al-mafazy, A.-W.; Ramsan, M.; Rotllant, G.; Gerstenmaier, J. F.; Molteni, F.; Abdulla, S.; Montgomery, S. M.; Kaneko, A.; Björkman, A. *PLoS Med.* **2007**, *4*, 1784–1790.
(7) http://www.who.int/malaria/docs/.
(8) Creek, D. J.; Charman, W. N.; Chiu, F. C. K.; Prankerd, R. J.; Dong, Y.; Vennerstrom, J. L.; Charman, S. A. *Antimicrob. Agents Chemother.* **2008**, *52*, 1291–1296.
(9) Singh, C.; Chaudhary, S.; Puri, S. K. *Bioorg. Med. Chem. Lett.* **2008**, *18*, 1436–1441.
(10) Whitty, C. J. M.; Rowland, M.; Sanderson, F.; Mutabingwa, T. K. *Br. Med. J.* **2002**, *325*, 1221–1224.
(11) White, N. J. *Science* **2008**, *320*, 330–334.
(12) *WHO: Facts on ACTs* (Artemisinin-Based Combination Therapies), Geneva, 2006.
(13) Pagola, S.; Stephens, P. W.; Bohle, D. S.; Kosar, A. D.; Madsen, S. K. *Nature* **2000**, *404*, 307–310.
(14) Egan, T. J. *Targets* **2003**, *2*, 115–124.
(15) Sahu, N. K.; Sahu, S.; Kohli, D. V. *Chem. Biol. Drug. Des.* **2008**, *71*, 287–297.
(16) Ziegler, J.; Linck, R.; Wright, D. W. In *Studies in Natural Products Chemistry*; Atta-ur-Rahman, Ed.; Elsevier Science B.V.: Amsterdam, 2001; Vol. 25, pp 327−366.
(17) Ridley, R. G. *Nature* **2002**, *415*, 686–693.
(18) Schwarzer, E.; Kühn, H.; Valente, E.; Arese, P. *Blood* **2003**, *101*, 722–728.
(19) Coban, C.; Ishii, K. J.; Sullivan, D. J.; Kumar, N. *Infec. Immun.* **2002**, *70*, 3939–3943.
(20) Jaramillo, M.; Godbout, M.; Olivier, M. *J. Immunol.* **2005**, *174*, 475–484.
(21) Riley, E. M.; Wahl, S.; Perkins, D. J.; Schofield, L. *Parasite Immunol.* **2006**, *28*, 35–49.
(22) Parroche, P.; Lauw, F. N.; Goutagny, N.; Latz, E.; Monks, B. G.; Visintin, A.; Halmen, K. A.; Lamphier, M.; Olivier, M.; Bartholomeu, D. C.; Gazzinelli, R. T.; Golenbock, D. T. *Proc. Natl. Acad. Sci. U.S.A.* **2007**, *104*, 1919–1924.
(23) Bohle, D. S.; Debrunner, P.; Jordan, P. A.; Madsen, S. K.; Schulz, C. E. *J. Am. Chem. Soc.* **1998**, *120*, 8255–8256.
(24) Sienkiewicz, A.; Krzystek, J.; Vileno, B.; Chatain, G.; Kosar, A. J.; Bohle, D. S.; Forrò, L. *J. Am. Chem. Soc.* **2006**, *128*, 4534–4535.
(25) Szaciłowski, K.; Macyk, W.; Drzewiecka-Matuszek, A.; Brindell, M.; Stochel, G. *Chem. Rev.* **2005**, *105*, 2647–2694.
(26) Gouterman, M. In *The Porphyrins: Physical Chemistry, Part A*; Dolphin, D., Ed.; Academic Press: New York, 1978; Vol. 3, pp 1−166.
(27) Adar, F. In *The Porphyrins: Physical Chemistry, Part A*; Dolphin, D., Ed.; Academic Press: New York, 1978; Vol. 3, pp 167−209.
(28) Adar, F.; Gouterman, M.; Aronowitz, S. *J. Phys. Chem.* **1976**, *80*, 2184–2191.
(29) Pope, M.; Swenberg, C. E. *Electronic Processes in Organic Crystals and Polymers*; 2nd ed.; Oxford University Press, Inc.: New York, 1999; Vol. 56.
(30) Kim, Y. H.; Jeong, D. H.; Kim, D.; Jeoung, S. C.; Cho, H. S.; Kim, S. K.; Aratani, N.; Osuka, A. *J. Am. Chem. Soc.* **2001**, *123*, 76–86.
(31) Boer, S. D.; Wiersma, D. A. *Chem. Phys. Lett.* **1990**, *165*, 45–53.
(32) Chen, J.-T.; Yu, Z.-X. *Appl. Phys. B: Laser Opt.* **1990**, *51*, 222–226.
(33) Monshouwer, R.; Abrahamsson, M.; Mourik, F. V.; Grondelle, R. v. *J. Phys. Chem. B* **1997**, *101*, 7241–7248.
(34) Harvey, P. D. In *The Porphyrin Handbook*; Kadish, K. M., Smith, K. M., Guilard, R., Eds.; Elsevier Science: New York, 2003; Vol. 18, pp 63−243.
(35) Mack, J.; Stillman, M. J. In *The Prophyrin Handbook*; Kadish, K. M., Smith, K. M., Guilard, R., Eds.; Elsevier Science: New York, 2003; Vol. 16, pp 43−116.
(36) Kasha, M. *Spectroscopy of the Excited State*; Plenum Press: New York, 1976.
(37) Kocka, J.; Stuchlick, J.; Stutzmann, M.; Chen, L.; Tauc, J. *Phys. Rev. B* **1993**, *47*, 13283–13294.
(38) Kale, R. B.; Sartale, S. D.; Chougule, B. K.; Lokhande, C. D. *Semicond. Sci. Technol.* **2004**, *19*, 980–986.
(39) Tauc, J.; Menth, A.; Wood, D. L. *Phys. Rev. Lett.* **1970**, *25*, 749–752.
(40) Petty, M. C. In *Molecular Electronics*; Capper, P., Kasap, S., Willoughby, A., Eds.; Wiley Interscience: New York, 2007; pp 65−128.
(41) Gutmann, F.; Lyons, L. E. *Organic Semiconductors*; John Wiley & Sons, Inc.: Sydney, Australia, 1967.
(42) Strickler, S. J.; Berg, R. A. *J. Chem. Phys.* **1962**, *37*, 814–822.
(43) Cohen, B.; Crespo-Hernandez, C. E.; Kohler, B. *Faraday Discuss.* **2004**, *127*, 137–147.
(44) Knorr, F. J.; Wall, M. H.; McHale, J. L. *J. Phys. Chem. A* **2000**, *104*, 9494–9499.
(45) Tauber, M. J.; Mathies, R. A. *J. Phys. Chem. A* **2001**, *105*, 10952–10960.
(46) Bhuiyan, A. A.; Seth, J.; Yoshida, N.; Osuka, A.; Bocian, D. F. *J. Phys. Chem. B* **2000**, *104*, 10757–10764.
(47) Park, M.; Cho, S.; Yoon, Z. S.; Aratani, N.; Osuka, A.; Kim, D. *J. Am. Chem. Soc.* **2005**, *127*, 15201–15206.
(48) Ishii, K.; Kobayashi, N. In *The Porphyrin Handbook*; Kadish, K. M., Smith, K. M., Guilard, R., Eds.; Elsevier Science: New York, 2003; Vol. 16, pp 1−42.
(49) Chou, J.-H.; Kosal, M. E.; Nalwa, H. S.; Rakow, N. A.; Suslick, K. S. In *The Porphyrin Handbook*; Kadish, K. M., Smith, K. M., Guilard, R., Eds.; Academic Press: New York, 2000; Vol. 6, pp 43−128.
(50) Bohle, D. S.; Kosar, A. D.; Stephens, P. W. *Can. J. Chem.* **2003**, *81*, 1285–1291.
(51) Granick, S.; Sassa, S.; Granick, J. L.; Levere, R. D.; Kappas, A. *Proc. Natl. Acad. Sci. U.S.A.* **1972**, *69*, 2381–2385.
(52) Lamola, A. A.; Yamane, T. *Science* **1974**, *186*, 936–938.
(53) Poh-Fitzpatrick, M. B.; Lamola, A. A.; Zalar, G. L.; Weinstein, M.; Doleiden, F.; Freeman, M. *J. Clin. Invest.* **1977**, *60*, 380–389.
(54) Poh-Fitzpatrick, M. B.; Lamola, A. A. *J. Lab. Clin. Med* **1976**, *87*, 362–370.
(55) Fischer, H. *Org. Syn.* **1955**, *3*, 442–443.
(56) Falk, J. E. *Porphyrins and Metalloporhyrins. Their General, Physical and Coordination Chemistry, and Laboratory Method*, BBA Library edition; Elsevier: Amsterdam, 1964; Vol. 2.
(57) Fuhrhop, J.-H.; Smith, K. M. In *Porphyrins and Metalloporphyrins*; Smith, K. M., Ed.; Elsevier Scientific: Amsterdam, 1975; p 869.
(58) Dixon, D. W.; Amis, L.; Kim, M. S.; Callahan, J. *J. Chromatogr.* **1989**, *462*, 411–418.
(59) Buffet, P. A.; Milon, G.; Brousse, V.; Correas, J.-M.; Dousset, B.; Couvelard, A.; Kianmanesh, R.; Farges, O.; Sauvanet, A.; Paye, F.; Ungeheuer, M.-N.; Ottone, C.; Khun, H.; Fiette, L.; Guigon, G.; Huerre, M.; Mercereau-Puijalon, O.; David, P. H. *Blood* **2006**, *107*, 3745–3752.
(60) Elliott, D. A.; McIntosh, M. T.; Hosgood, H. D.; Chen, S.; Zhang, G.; Baevova, P.; Joiner, K. A. *Proc. Natl. Acad. Sci. U.S.A.* **2008**, *105*, 2463–2468.

(61) Karl, S.; David, M.; Moore, L.; Grimberg, B. T.; Michon, P.; Mueller, I.; Zborowski, M.; Zimmerman, P. A. *Malar. J.* **2008**, *7*, 66.
(62) Schwarzer, E.; Bellomo, G.; Giribaldi, G.; Ulliers, D.; Arese, P. *Parasitology* **2001**, *123*, 125–131.
(63) Nagababu, E.; Rifkind, J. M. *Biochem. Biophys. Res. Commun.* **1998**, *247*, 592–596.
(64) Carney, C. K.; Schrimpe, A. C.; Halfpenny, K.; Harry, R. S.; Miller, C. M.; Broncel, M.; Sewell, S. L.; Schaff, J. E.; Deol, R.; Carter, M. D.; Wright, D. W. *J. Biol. Inorg. Chem.* **2006**, *11*, 917–929.
(65) Wood, B. R.; Langford, S. J.; Cooke, B. M.; Lim, J.; Glenister, F. K.; Duriska, M.; Unthank, J. K.; McNaughton, D. *J. Am. Chem. Soc.* **2004**, *126*, 9233–9239.
(66) Wood, B. R.; Langford, S. J.; Cooke, B. M.; Glenister, F. K.; Lim, J.; McNaughton, D. *FEBS Lett.* **2003**, *554*, 247–252.
(67) Mukamel, S. *Annu. Rev. Phys. Chem.* **2000**, *51*, 691–729.
(68) Akins, D. L.; Zhu, H.-R.; Guo, C. *J. Phys. Chem.* **1994**, *98*, 3612–3618.
(69) Akins, D. L.; Özçelik, S.; Zhu, H.-R.; Guo, C. *J. Phys. Chem.* **1996**, *100*, 14390–14396.
(70) Purrello, R.; Gurrieri, S.; Lauceri, R. *Coord. Chem. Rev.* **1999**, *190*−*192*, 683–706.
(71) Purrello, R.; Raudino, A.; Scolaro, L. M.; Loisi, A.; Bellacchio, E.; Lauceri, R. *J. Phys. Chem. B* **2000**, *104*, 10900–10908.
(72) Peng, X.; Huang, J.; Ji, L. *Chin. Sci. Bull.* **2000**, *45*, 418–421.
(73) Zhang, Z.; Nakashima, K.; Verma, A. L.; Yoneyama, M.; Iriyama, K.; Ozaki, Y. *Langmuir* **1998**, *14*, 1177–1182.
(74) Burrows, H. D.; Gonsalves, A. M. R.; Leitao, M. L. P.; Miguel, M. d. G.; Pereira, M. M. *Supramol. Sci.* **1997**, *4*, 241–247.
(75) Terenin, A.; Putzeiko, E.; Akimov, I. *Discuss. Faraday Soc.* **1959**, *27*, 83–93.
(76) Vartanyan, A. T. *USSR. Izv. Vyssh. Uchebn. Zaved., Khim. Khim. Tekhnol.* **1986**, *29*, 3–15.
(77) Bélisle, J. M.; Costantino, S.; Leimanis, M. L.; Bellemare, M.-J.; Bohle, D. S.; Georges, E.; Wiseman, P. W. *Biophys. J.* **2008**, *94*, L26−L28.
(78) Lwin, K. M.; Ashley, E. A.; Proux, S.; Silamut, K.; Nosten, F.; McGready, R. *Malar. J.* **2008**, *7*, 57–62.
(79) Bellemare, M.-J.; Bohle, D. S. *Inorg. Synth.* **2009**, submitted for publication.
(80) Trager, W.; Jenson, J. B. *Nature* **1978**, *273*, 621–622.
(81) Lambros, C.; Vanderberg, J. P. *J. Parasitol.* **1979**, *65*, 418–420.
(82) Radzioch, D.; Hudson, T.; Boulé, M. L. B.; Urbance, J. W.; Varesio, L.; Skamene, E. *J. Leukoc. Biol.* **1991**, *50*, 263–272.
(83) Killick-Kendrick, R.; Peters, W. *Rodent malaria*; Academic Press: London, 1978.

JP8104375